This manuscript has been submitted for publication in **Water Resources Research**. Please note that, despite having undergone peer-review, the manuscript has yet to be accepted for publication. Subsequent versions of this manuscript may have slightly different content. If accepted, the final version of this manuscript will be available via the 'Peer-reviewed Publication DOI' inside of this webpage. Please feel free to contact any of the authors; we welcome feedback.

Comparison of estimation methods for a nonstationary index-flood model in flood frequency analysis using peaks over threshold

Martin Durocher[1,*], Donald H. Burn[1] and Fahim Ashkar[2].

1 - University of Waterloo, Department of Civil and Environmental Engineering, Waterloo (ON), Canada, N2L 3G1.

2 - University of Moncton, Department of Mathematics and Statistics, Moncton (NB), Canada, E1A 3E9

* - Corresponding author: mduroche@uwaterloo.ca

Keywords: Canada, Floods, Nonstationarity, Peaks over threshold, Regional Frequency Analysis.

Abstract

Due to climatic or anthropogenic causes, changes in flood magnitudes in many parts of the world have been observed and are expected to continue in the future. To characterize such changes, nonstationary models have focussed on the modeling of stations with long records, but in practice such models may be needed to improve the evaluation of flood risk for stations having shorter records. In this study, a nonstationary index-flood model for peaks over threshold is investigated to reduce model uncertainty in such situations. A procedure is proposed to automatically calibrate such models for at-site and regional frequency analysis. The assumption of an index-flood model is used to define a probability structure that is stable in time. This requires adapting existing automatic procedures for threshold selection and the delineation methods for forming pooling groups to the nonstationary models. Four estimators are investigated in a simulation study to determine which perform best in different situations. Two methods are based on the combination of regression techniques and L-moments, while the other two methods employ likelihood-based

techniques. A case study of 425 stations in Canada is considered to verify if a nonstationary index-flood model using pooling groups that combine stationary and nonstationary stations can reduce the uncertainty of design levels associated with a finite reference period.

1. Introduction

The evaluation of risk associated with flood events is an important factor in the design of safe and reliable infrastructure. In particular, estimation of accurate flood quantiles is challenging as it requires the extrapolation of the tail of a probability distribution estimated from a limited number of extreme events. To increase the amount of information, threshold models were introduced as an alternative to the more common strategy of modeling annual maximum discharges. Comparative studies showed that this strategy, which allows the inclusion of more than one peak per year, can effectively reduce model uncertainties (Bezak et al., 2014; Madsen et al., 1997), although the efficiency of threshold methods may vary, based on factors such as the number of peaks per year (Cunnane, 1973). Another strategy to reduce model uncertainty in flood frequency analysis is to include information from nearby stations with similar hydrological properties. Such an approach, called regional frequency analysis, is often recommended by governmental authorities to perform frequency analysis on stations having few years of data (Robson and Reed, 1999; USGS, 2018). Among popular regional approaches, the index-flood model is widely applied (Hosking and Wallis, 1997; Ilorme and Griffis, 2013; Nobert et al., 2014; Wright et al., 2014). The latter assumes that every station inside a homogenous group has the same regional distribution (or growth curve) up to a scale factor. This hypothesis proved to be a flexible approach that led to various generalizations, such as multivariate frequency analysis of peaks and volumes (Chebana and

Ouarda, 2009; Requena et al., 2016) and spatial extremes characterized by max-stable processes (Wang et al., 2014) .

There is evidence that changes in flood regimes are occurring due to either climatic (Burn et al., 2016; Kiem et al., 2003; Kundzewicz, 2012) or anthropogenic causes (Prosdocimi et al., 2015; Villarini et al., 2009). Distinguishing between long-term persistence and short oscillation patterns in environmental time series represents an important dilemma that affects the interpretation of the observed changes. Some authors pointed out that stationary time series may possess persistence in the data, even though the probability structure of the studied phenomenon does not change (Koutsoyiannis, 2005; Montanari and Koutsoyiannis, 2014). Consequently, research that has addressed the issues related to change in flood regimes has mostly focussed on analysis with long records to characterize and attribute changes to specific drivers (Blöschl et al., 2007; Hall et al., 2014; Mediero et al., 2015). Some studies have considered regional approaches to attribute changes in flood regimes (Renard and Lall, 2014; Sun et al., 2014), but such approaches remain relatively marginal and changes are generally investigated for a specific station (Viglione et al., 2016). In a nonstationary frequency analysis, the major challenge remains to adequately predict trends. Recent studies demonstrate that even when stations present significant signs of nonstationarity, the variability of the trends estimated using uniquely time as covariate are still too important for nonstationary models to provide a valuable replacement to existing stationary models (Renard et al., 2013; Serinaldi and Kilsby, 2015). Indeed, even a simple linear trend can diverge considerably from the truth over the years. As a compromise, Luke et al. (2017) recommended in the United States the approach of updated stationarity where the predicted trend is constant and equal to the last observed year. This provides a balance between opting for a stationary model that ignores the observed trend and a nonstationary model that leads to an unrealistic flood estimate.

To adapt flood frequency models to nonstationary situations, a common approach is to let the parameters of extreme distributions evolve as a function of temporal covariates (El Adlouni et al., 2007; Katz, 2013; Villarini et al., 2010). Similarly, it was shown that using common regression models applied to the logarithm of annual maximum floods were proper methods to describe the trends observed in most watersheds in the United States (Serago and Vogel, 2018; Vogel et al., 2011). Additionally, several studies for modeling peaks over threshold have also considered a time-dependent threshold to ensure that the exceedance probability remains constant in time (Kyselý et al., 2010; Northrop and Jonathan, 2011). A nonstationary index-flood model for extreme rainfall was presented by Hanel et al. (2009) in the case of annual maxima and by Roth et al. (2012) in the case of peaks over threshold. The main innovation was the introduction of a time-dependent scaling function to replace the constant scale factor. This modification created growth curves that are stable in time and thus can be unique inside a homogenous region. Moreover, they suggested a further generalization that lets the parameters of the regional growth curve vary in time to describe temporal trends common to the homogenous region. For modeling flood peaks over a given threshold, Madsen and Rosbjerg (1997) investigated a procedure to estimate a stationary index-flood model based on L-moments. Their methodology estimates a regional shape parameter of the Generalized Pareto distribution (GPA) using L-coefficient of variation and the scale parameter was taken as the at-site mean. Contrary to Roth et al. (2012) that used the threshold as a scaling function, a generalization of the Madsen and Rosbjerg (1997) model involves using a time-dependent mean excess function. The direct correspondence between the mean excess and the scale parameter of the GPA distribution implies an equivalent representation, but with a clearer separation of the time-dependent component (mean excess) and the probabilistic structure (growth curve). O'Brien and Burn (2014) applied a nonstationary index-flood model to the estimation of flood quantiles in Canada using the annual maximum of river discharges that, contrary to Hanel et al. (2009), used a constant scaling factor and a time-dependent growth curve. Their study reveals an additional challenge in the application of regional and nonstationary flood frequency analysis, because tests for trend applied on a large network of gauged stations resulted in a limited number of stations presenting significant signs of nonstationarity. The scarcity of the nonstationary stations restricted the availability of nearby sites having similar hydrological properties, which complicated the formation of the homogenous regions.

Homogenous regions can be formed following the notion of regions of influence, which was demonstrated to lead to more accurate estimates of flood quantiles than fixed regions (Burn, 1990; GREHYS, 1996; Tasker et al., 1996). A region of influence entails the formation of pooling groups that include the stations nearest to a target site. A particularity of this delineation method is that the pooling groups are specific to a target and the same station can be part of two pooling groups having similar but different growth curves. Consequently, the rationale of combining the region of influence methodology with index-flood models is to obtain a neighborhood of similar stations where the global probability structure can be locally approximated by a unique growth curve. Another important aspect for modeling exceedances is the selection of a proper threshold. A threshold should normally be selected as low as possible, while respecting the model assumptions. In this regard, an important aspect for selecting a threshold is the notion of stability that entails that if GPA is a proper model for the exceedances of a given threshold, then the exceedances of a higher threshold should also follow a GPA distribution with the same shape parameter (Coles, 2001). An indicator for determining if a threshold was correctly selected is to use a goodness-of-fit test to verify that GPA is a proper distribution (Davison and Smith, 1990). The p-value of such tests were used recently to develop automatic selection procedures based on the identification of the maximum p-value and the first threshold respecting a given significance level (Durocher et al., 2018b; Solari et al., 2017).

The objective of the present study is to propose an automatic procedure to perform the calibration of a nonstationary index-flood model for peaks over threshold. In addition to testing for trends in the frequency of occurrences and magnitudes of the threshold exceedances, the methodology includes a way of selecting the time-dependent threshold and mean excess function. More precisely, this procedure involves using the stability of the growth curve to adapt existing methods to nonstationary models. It also allows the formation of pooling groups that combine stationary and nonstationary stations to maximize the information provided by the nearby stations. In at-site flood frequency analysis, L-moments are often preferred for curve fitting, to the alternative method of maximum likelihood, due to their robustness and lower bias (Hosking, 1990; Madsen et al., 1997). Similarly, the proposed procedure suggests a methodology based on regression techniques and L-moments. The relative performance of this estimation method is compared to existing likelihood-based methods to identify the best method for different circumstances. The present study does not address the task of forecasting trend, which demands a separate focused attention. The focus is rather put on a methodology that could be applied in practice and that can improve flood quantile estimates for stations having limited data and for which nonstationarity is suspected. According to the idea of update stationarity (Luke et al., 2017), there is interest in investigating flood quantiles of the most recent years, as they may be among the best indicators of future flood risk. Consequently, this study attempts to put forward models that reduce the uncertainties of design levels that summarize flood risks over the most recent year of observation (Cooley, 2013; Salas et al., 2018).

The investigated model has 3 important components: the threshold, the mean excess series and the growth curve. Section 2 explains these components in more detail and presents the stepwise procedure for calibrating the model. For simplicity, time is used as a predictor (covariate), but this could be replaced by other meaningful descriptors. Section 3 provides a simulation study that compares the relative performance of four estimators including 2 at-site and 2 regional ones. In section 4, a case study based on 425 stations in Canada is used to verify that the regional version of the proposed method can reduce the uncertainty of estimated design levels in comparison to existing at-site methods. Finally, Section 5 discusses the results and draws conclusions.

2. Methodology

2.1 Model components

Let's consider first the modeling of a single station. Stationary threshold models assume that the probability of exceeding the threshold is constant through time. When this hypothesis is unrealistic, quantile regression is suggested to define a time-dependent threshold that restores a constant probability of exceeding the threshold (Kyselý et al., 2010; Northrop and Jonathan, 2011). Quantile regression estimates conditional quantiles with respect to covariates without choosing a specific distribution to fit to the data (Koenker and Bassett, 1978). For streamflow data, a declustering method is necessary to identify independent peaks from a series of daily river discharge. To this end, the declustering method recommended by the Water Resource Council of the United States as described in Lang et al. (1999) is applied. In brief, two adjacent peaks must respect the following two conditions: i) they must be separated by $4+\log(A)$ days, where A is the drainage area in square kilometers; and ii) the minimal intermediate flow must be less than 75% of the lowest of the two peaks. Utilization of a declustering method creates a discrepancy between the exceedance probability of the peaks and the probability associated with the conditional quantile of the quantile regression. For this reason, the exceedance probability is estimated as the ratio n/N representing the extracted number of peaks divided by the number of daily observations (Coles, 2001). Henceforth, let $u_\lambda(t) = a_0 + a_1 t$ be a time-dependent threshold associated with a rate λ representing the average number of peaks per year (PPY). Note that this rate is proportional to the exceedance probability, the proportionality factor being the number of days in a year (365.25) and has comparable interpretation in both stationary and nonstationary models.

The second component of the model is the mean excess that can be constant or time-dependent. In the latter case, it describes a trend in the magnitude of the exceedances. Let $Y(t)$ be a random variable characterizing exceedances. Based on theoretical arguments, $Y(t)$ follows a Generalized Pareto (GPA) distribution (Davison and Smith, 1990)

$$F(y) = 1 - \exp\left(-\frac{y}{\alpha}\right), \quad \kappa = 0$$
$$F(y) = 1 - \left(1 - \frac{\kappa}{\alpha} y\right)^{1/k}, \quad \kappa \neq 0 \tag{1}$$

where $\alpha > 0$ is the scale parameter and κ is the shape parameter. The mean excess and the excess variance are related to these GPA parameters by the relationship

$$\mu = \frac{\alpha}{1+\kappa} \quad \text{and} \quad \sigma^2 = \frac{\alpha^2}{(1+\kappa)^2 (1+2\kappa)}. \tag{2}$$

If the GPA shape parameter κ is constant, equation (2) implies that the mean excess and the scale parameter are proportional up to a scaling factor depending on κ. This means that when they are time-dependent both share a similar nature. For instance, if the mean excess $\mu(t)$ is linear, so is the scale parameter $\alpha(t)$.

The third component of the model is a dimensionless growth curve that describes the probability structure of the exceedances. Using the mean excess as a scaling factor leads to the definition of the standardized exceedance $Z(t) = Y(t) / \mu(t)$, which has $E\left[Z(t)\right] = 1$ and follows a distribution $\mathrm{GPA}\left(1+\kappa, \kappa\right)$ controlled uniquely by the shape parameter κ. Note that the representation using the mean excess and the growth curve is equivalent to directly using the shape parameter of the GPA model. However, the proposed methodology appears more straightforward when using this form.

When the model is applied in a regional analysis, it can be assumed that all stations inside a homogenous region have the same (regional) growth curve, which is the assumption of an index-flood model (Hosking and Wallis, 1997). A further generalization is introduced by considering a space-dependent GPA shape parameter related to a linear predictor

(3) $$\kappa(s) = \mathbf{x}(s)'\beta,$$

where s is the station of interest, β is a vector of parameters and $\mathbf{x}(s)$ a vector of descriptors. Overall, for a station s the proposed model evaluates the flood quantile of probability p at a specific time t as

(4) $$Q_{s,p}(t) - u_{s,\lambda}(t) = \mu_s(t) \times q_p(s),$$

where $q_p(s)$ is a growth curve, $u_{s,\lambda}(t)$ is the station threshold and $\mu_s(t)$ is the station mean excess. The choice of using a linear predictor that depends on station characteristics is made to provide a clear separation between the temporal and spatial components of the model.

2.2 Automatic calibration procedure for one station

The nonstationary model is calibrated following an automatic procedure that verifies the model hypothesis in a stepwise manner. A simple automatic procedure to determine the threshold u_λ consists of selecting the largest threshold for which a goodness-of-fit test, such as the Anderson-Darling (AD), cannot reject the hypothesis of a GPA distribution (Davison and Smith, 1990). Considering a set of candidate thresholds, one can iterate until the p-value of the goodness-of-fit test is greater than a chosen value. This significance-based strategy was criticized because it fails in some situations to provide a stable threshold based on common visual diagnostics. As a solution, Solari et al. (2017) showed that a proper alternative is to use the threshold that leads to the maximum p-value of the goodness-of-fit test. A comparison of these two approaches was later performed by Durocher et al. (2018b). They noticed that the significance-based method fails in a limited number of cases and that when it doesn't fail, it leads to models with lower uncertainty. They also found that a large discrepancy between the flood quantile of a candidate threshold and the one of a lower reference threshold provides a good indicator of failures. This resulted in the proposition of a hybrid procedure where an alternative method to the significance-based method is preferred only when the discrepancy is considered large enough to suggest that stability has not been reached. In this study, a set of 30 candidate thresholds between 0.8 and 2.5 PPY are identified by an initial screening process. The significance-based and the maximum p-value thresholds are then searched among the candidates and the final threshold is taken as the one with the highest number of peaks. In particular, the significance-based threshold is chosen as the first threshold that has a p-value greater than 0.25 and a relative discrepancy with the 1 PPY threshold lower than 25%. To speed up the computation, a table is used to interpolate the p-values of the Anderson-Darling test (Choulakian and Stephens, 2001). Although this table does not allow the evaluation of p-values greater than 0.5, it was shown that such restriction does not substantially affect the performance of the two automatic procedures (Durocher et al., 2018b).

Once the exceedances are extracted, a logistic regression model is applied to identify the presence of a significant trend in the occurrences of peaks (Frei and Schär, 2001). If the slope is not significant, the threshold is assumed to be constant; otherwise a time-dependent threshold is added to the model. The same automatic selection procedure is therefore repeated using quantile regression to identify the exceedances. Afterward, the hypothesis of a time-dependent mean excess function is verified by the Mann-Kendall test (Helsel and Hirsch, 2002). To account for possible temporal correlation, block bootstraps are employed to obtain a more robust evaluation of the significance level (Önöz and Bayazit, 2012). If a trend in the magnitude of the exceedances cannot be rejected, a time-dependent mean excess function is added. At this point, the automatic selection procedure cannot be used directly, because the goodness-of-fit test is not applied on identically distributed data. The reformulation of the GPA distribution in terms of a growth curve scaled by the mean excess function becomes useful as the automatic procedure can be applied on the standardized exceedances. In this context, the automatic procedure ensures that the growth curve has reached stability for the selected threshold.

2.3 Estimation of the mean excess and growth curve

The generalized linear model (GLM) extends the classical linear model by considering alternative distributions to the Normal distribution. In particular, GLM includes a variance function $V(\mu)$ that characterizes the model variance $\sigma^2 = \phi V(\mu)$ in respect of the mean μ, up to a dispersion parameter ϕ. Equation (2) shows that the mean excess $\mu(t)$ can be estimated as a GLM model where the variance function is the square function $V(\mu) = \mu^2$ and the dispersion parameter

$\phi = 1/(1+2\kappa)$ depends on the GPA shape parameter κ. In that context, κ is treated as a nuisance parameter in the sense that it is not needed to estimate the mean. The quasi-likelihood approach is an estimation method that mimics the properties of the maximum likelihood approach, but uses only the information from the first two moments. For this study, the mean excess has the form

$$\mu(t) = g\left(b_0 + b_1 t\right) \tag{5}$$

where $\mathbf{b} = \left(b_0, b_1\right)$ is a vector of parameters and g is a link function that relates the mean excess to a linear predictor. Here, the link function is restricted to a constant or an exponential function; where the latter may be useful to enforce positive values. For exceedances $\mathbf{y} = (y_1, ..., y_n)$ observed at time $\mathbf{t} = (t_1, ..., t_n)$, the quasi-likelihood function has the form

$$h(\mathbf{b}; \mathbf{z}) = \sum_{i=1}^{n} \left[-\frac{y_i}{\mu(t_i)} - \log \mu(t_i) \right] \tag{6}$$

and plays a similar role to the log-likelihood function that can be minimized to obtain an estimate of the model parameters. An important part of the assessment of a regression model is the examination of the residuals. Here, the (Pearson) residuals are generally skewed and do not provide the same intuitive diagnostic. For a GLM model with squared variance function, the deviance residuals

$$e_i = \operatorname{sign}(y_i - \hat{y}_i) \sqrt{2\left[\frac{y_i - \hat{y}_i}{\hat{y}_i} - \log\left(\frac{y_i}{\hat{y}_i}\right) \right]} \tag{7}$$

follow approximately a standard Normal distribution and are more appropriate for visualization. Please see McCullagh and Nelder (1989) for a more in-depth introduction of GLM modeling.

Once the threshold and mean excess of the model are estimated, empirical values of the standardized exceedances can be computed. Using only at-site information, one possible estimator for the GPA shape parameter κ of the growth curve is the L-moment estimator

(8) $$\hat{\kappa} = \frac{1}{\hat{\tau}} - 2$$

where $\hat{\tau}$ is the empirical estimate of the L-coefficient of variation (Madsen and Rosbjerg, 1997).

2.4 Formation of the pooling groups

In this study, the pooling groups are built using a hierarchical structure that accounts for more than one notion of similarity. Similar strategies were proposed, for instance, by Eng et al. (2007) and Durocher et al. (2018a). First, the m_0 nearest stations to the target are identified according to geographical distance. Then, among the identified stations, the final m stations are selected as the most similar to the target in terms of seasonality. Mostafi Zadeh et al. (2019) indicated that regional frequency analysis performed with pooling groups based on a seasonality measure using annual maximums are more accurate than a seasonality measure based on peaks over threshold. In the seasonality space, a station can be represented as a circular statistic (θ, r), where θ characterizes the average date on which the annual maximum occurs (in degrees) and $r \in [0,1]$ measures the regularity of this annual maximum event. For instance, $r = 1$ and $\theta = 180^\circ$ would imply that the largest flood events happen every year on July 1st. The adopted seasonality measure is

(9) $$\|(\theta_1, r_1) - (\theta_2, r_2)\|^2 = \left(\frac{\min\{\Delta, 360 - \Delta\}}{180} \right)^2 + (r_1 - r_2)^2 .$$

where $\Delta = |\theta_1 - \theta_2|$.

From the steps described in Section 2.3, at-site estimates of the GPA shape parameter $\hat{\kappa}_j$ can be obtained for each station s_j of a pooling group. The drainage area (AREA) and mean annual precipitation (MAP) defines the linear predictor, Equation (3), that characterizes the relationship between the GPA shape parameter and its descriptors. To reduce skewness and impose a scale for comparison, both descriptors are initially transformed using the logarithm function and standardized. A GLM model assuming a Normal distribution is employed to estimate the parameter β of the linear predictor, Equation (3). To find appropriate neighborhood sizes, the objective is to determine $m_0 > m$ such that the pooling groups best predict the target GPA shape parameter, which is accomplished by leave-one out cross-validation. In turn, the GPA shape parameter $\hat{\kappa}_{(i)}$ of the target station is predicted as if it was ungauged. This process is repeated for every pooling group and the cross-validation score

$$C = \sqrt{\frac{1}{m}\sum_{j=1}^{m}\left(\hat{\kappa}_j - \hat{\kappa}_{(j)}\right)^2} \tag{10}$$

is evaluated. The best combination (m_0, m) is determined as the one with the lowest cross-validation score. To limit the search of all possible combinations, the candidate sizes are limited to multiples of 5 for m and to multiples of 25 for m_0.

2.5 Likelihood-based method

Sections 2.3 and 2.4 indicate how the mean excess and growth curve of a nonstationary index-flood model can be estimated using L-moments and regression techniques. An alternative to this stepwise method is to directly use the likelihood of the model. Following the adopted notations, the parameter of the nonstationary index-flood model can be written

$$\begin{aligned}\kappa(s) &= \mathbf{x}(s)'\beta \\ \alpha(t) &= g(b_0 + b_1 t)\times\left[1+\kappa(s)\right]\end{aligned} \quad . \tag{11}$$

For at-site frequency analysis, the GPA shape parameter is constant $\kappa(s) = \kappa$ and the likelihood function $L(\mathbf{b}, \kappa; \mathbf{y})$ can be used to obtain the maximum likelihood estimator. Afterward, using the properties in Equation (2), the mean excess and the growth curve can be derived from the estimated parameters.

Although dependence structure and estimation methods exist for modeling spatial extremes (Davison et al., 2012; Padoan et al., 2010; Thibaud et al., 2013), when the focus is the quality of the fitted distribution and not the realism of the simulations, simpler estimation methods were shown to lead to proper inference without specifying such dependence structure. One approach is the independent likelihood method that optimizes jointly the likelihood of multiple stations as if all stations were independent (Roth et al., 2012; Wang et al., 2014). Let $\mathbf{y}_j$ be the exceedances of the station s_j inside a pooling group of size *m* and $(\mathbf{b}_j, \beta)$ the model parameters associated with station j. Accordingly, the likelihood of the jth station is $L(\mathbf{b}_j, \beta; \mathbf{y}_j)$ and the independent likelihood of the multi-station model is simply

$$L(\mathbf{b}_1, \dots, \mathbf{b}_m, \beta; \mathbf{y}_1, \dots, \mathbf{y}_m) = \prod_{j=1}^{m} L(\mathbf{b}_j, \beta; \mathbf{y}_j) \; . \tag{12}$$

The maximization of the independent likelihood is sometimes challenging. Here, the algorithm is initialized using the parameters estimated by the regression approach and follows the procedure described in Roth et al. (2012). In brief, it alternates between a phase where the growth curve is optimized assuming the mean excess of all stations is known and a phase where the at-site estimation of each station is optimized separately assuming that the growth curve is known.

Asymptotic results for the distribution of the parameters estimated by the independent likelihood method are presented, for instance, in Varin et al. (2011). However, the present study relies on a parametric bootstrap method to quantify the uncertainty of the model because the same method can be applied to the regression approach. In particular, bootstraps are necessary to propagate the error made at each step of the methodology. The resampling scheme includes an adjustment for intersite correlation by using simulations generated from a multivariate Normal distribution with constant coefficient of correlation (Hosking and Wallis, 1997). Contrary to regional models using annual maximums, peaks over threshold events are not observed at regular time steps. Consequently, it is assumed that correlation only affects pairs of exceedances separated by less than a month and the dependence parameter is estimated as the average correlation coefficient. The multivariate simulations are transformed to GPA distributions using the parameters obtained by the at-site estimation of each station by the combination of regression techniques and L-moments.

2.6 Evaluation of flood risk

For a stationary model, flood risk is measured in terms of a return period, T, corresponding to the expected waiting time before the occurrence of an event of similar magnitude. For threshold models, a return period is associated with the quantile of the GPA distribution having probability $p_T = 1-(\lambda T)^{-1}$, where λ corresponds to the mean number of peaks per year (Madsen and Rosbjerg, 1997). For nonstationary models, a different flood quantile is evaluated each year and the usual correspondence between exceeding probability and expected waiting time does not hold. In practice, a generalization of expected waiting time to a nonstationary model is more challenging, because to evaluate the expected waiting time of a 100 year return period, it is necessary to know the trends for a period longer than 100 years (Cooley, 2013). This can be especially problematic considering that accurate prediction of future trends remains an open problem in flood frequency analysis (Luke et al., 2017; Serinaldi and Kilsby, 2015).

Measuring risk as a probability associated with a finite reference period is simpler. The reliability associated with a given design level is defined as the probability that no event of such magnitude occurs during this period. The probability of failure is then one minus the reliability. If $p_i(z) = \Pr\left[Z(t_i) < z\right]$ denotes the probability of not surpassing the design level z during year t_i, then the reliability over a reference period of r years is defined as

(13) $$R = \prod_{i=1}^{r} p_i(z)$$

The design level z can be deduced numerically by solving the above equation for the desired level of reliability R (Salas et al., 2018). As defined in Equation (13), the reliability makes the approximation that the exceedance probabilities $p_i(z)$ are constant during a year. For this study, the probabilities $p_i(z)$ are based on the yearly evaluation of the growth curve on July 1st.

To better understand the severity of a flood associated with a given reliability level, note that the reliability of a stationary model is p_T^r. For instance, the reliability of a 100 year return period over 30 years and having $\lambda = 2.5$ is R = 0.887. Accordingly, a convention is adopted to report flood severity in terms of a design level having a reliability equivalent to a flood quantile of a T year return period in a stationary model. In particular, the design level Q10 and Q100 are having the reliability level $\left[1-(\lambda T)^{-1}\right]^r$ where T = 10 and 100. Following this definition equivalent to a T year return period, simple calculation shows that

(14) $$\log(p_T) = \frac{1}{r}\sum_{p=1}^{r} \log p_i(z),$$

which means that the design level used in this study represents a central tendency measure of the flood quantiles of respective return periods during the period of reference.

3. Simulation study

A simulation study is performed to evaluate the relative performance of the regression versus the likelihood-based approach for estimating the parameters of the nonstationary index-flood model. Both at-site and regional models are considered. The comparison is based on a target station simulated with a homogeneous group formed of 20 similar stations that are identically and independently distributed. The notation LMM is used to denote the at-site method using the combination of regression techniques and L-moments (section 2.3). Similarly, the RLM method represents the regional version of the LMM method, where the GPA shape parameter is estimated by a second regression model (Section 2.4). The MLE method corresponds to the at-site maximum likelihood estimator and the IND method is the method using an independent likelihood method that jointly fits the 20 stations assuming a constant regional GPA shape parameter (Section 2.5).

Among many factors, the quality of the estimation method will be affected by the number of peaks. Here, an average of two peaks per year is assumed across the simulation study and the record lengths considered are n = 30, 50 and 100 years. The time of observation for each exceedance is selected at random in the interval [0, n]. For every experiment, the threshold is zero and assumed to be known. The mean excess is defined as a linear trend that is one at the origin and has a 1% annual increase. Every experiment is repeated 1000 times for several GPA shape parameters, κ, ranging from -0.3 to 0.3 by steps of 0.1.

The accuracy of some model components is summarized using bias and root mean square error (RMSE). Figure 1 reports the RMSE of the shape, slope and design level (flood quantile) Q100 for the different simulated GPA shape parameters. Note that Q100 is based on the last 30 years of simulated data. As expected, the third row shows that the regional methods are more accurate than the at-site methods. In particular, the IND method is found to be systematically the best method for predicting Q100. However, the differences between RLM and IND are relatively small, in particular for simulated GPA shape parameters between -0.1 and 0.1. The differences outside this range seem to mostly result from lower accuracy in the estimation of the linear trend because the RMSE of the GPA shape parameter for the IND method is not systematically better than the RMSE for RLM. Note that in the second row of Figure 1, RLM and LMM have the same estimated slope and thus the difference of accuracy is a consequence of the approach used for the estimation of the GPA shape parameter. In terms of bias, which is represented in Figure 2, the first row of this figure indicates that the RLM has smaller bias than the IND method for GPA shape parameters lower than -0.1. This difference in bias performance between the methods also translates to lower bias for Q100.

The comparison of the at-site methods also has a special interest as the procedure proposed to guide the choice of the time-dependent components is based only on the data of the target station. Figure 1 indicates lower RMSE in the GPA shape parameter and design level Q100 for the LMM method in comparison to the MLE method when simulations are performed using negative GPA shape parameters and 30 or 50 years of simulations. This conclusion suggests that LMM is more robust in the sense that it is better at estimating the GPA shape parameters of smaller samples with heavy tails, which impact the accuracy of Q100. MLE performs relatively better when simulations have positive GPA shape parameters and more data. When looking at the bias in Figure 2, both estimation methods tend to overestimate the GPA shape parameter, but LMM is found to be less biased. In particular, as the GPA shape parameter becomes more positive, LMM becomes relatively less biased, while MLE becomes more biased. The same conclusion applied to Q100, even though bias remains relatively small. By comparison, the design level associated with a GPA shape parameter of zero is 4.6 and the highest relative bias of MLE for Q100 is 2%. Overall this shows that using the LMM approach for calibration is a safer approach because when the RMSE is large (heavy tails) it provides a gain of accuracy and when RMSE is small (light tails) it is less biased. Section 2.5 described the parametric bootstrap procedure used to evaluate the uncertainty of the four estimators. For that resampling scheme, the LMM estimate is used as plug-in value to transform the marginal distribution. This choice can be motivated by the relatively lower bias compared to the likelihood-based estimator.

Other experiments were performed, but detailed results are not reported. In particular, the impact of including intersite correlation using a multivariate Normal distribution with constant correlation coefficient was considered. Increasing the intersite correlation did decrease the overall accuracy of all methods, but did not affect the relative performance of the four estimation methods. Adding a small perturbation to the GPA shape parameter was also considered, but again none of the estimators performed relatively better than the others under this type of model misspecification.

4. Case study

4.1 Data and local trends

The Water Survey of Canada (WSC, 2018) manages a large network of gauge stations that provide daily measurements of streamflow across the country. For the purpose of this study, a total of 425 stations are selected that have unregulated streamflows and at least 27 years of complete data during the reference period of 1988 and 2017. This reference period of thirty years was selected because it represents a common window to evaluate persistence in climate data and it is used to evaluate design levels. Furthermore, it ensures a minimal record length for each station and a good representation of the trend during the reference period. Table 1 presents a contingency table that describes the properties of the selected stations. Approximately half of the selected stations (215) have between 40 and 60 years of streamflow data, 134 stations have less than 40 years and 76 stations have more than 60 years. Figure 3 presents the locations of the selected stations. Notice that the criteria used for selecting the stations creates a selection bias where stations located in the Prairies and the northern regions are relatively few.

Burn et al. (2016) investigated changes in peaks over threshold data in Canada using a classification based on three types of flood regimes. A similar approach is adopted herein, where hierarchical clustering (Ward, 1963) is applied to define seasonality regions using the seasonality measure of Equation (9). Figure 4 illustrates the locations and seasonal properties of 6 clusters. The average monthly maximum flow of each station is computed to create a profile vector that offers a second representation of the flood seasonality. To account for catchment scale, every profile vector is standardized to a unit norm. The two panels at the bottom of Figure 4 present respectively the average profile vector of each cluster and the locations of the stations in seasonality space. Cluster 5 is found mostly along the Pacific coast and is mostly associated with a pluvial regime in the sense that flood peaks are not dominated by an annual snowmelt event (see average monthly maximum flow). Cluster 6 contains mainly high elevation and high latitude stations that are associated with nival regimes where snowmelt occurs gradually and later during the summer. In southern Ontario and the Atlantic provinces, stations with mixed regimes are observed. Their main flood peaks are during spring, but also have important flood events occurring during fall and winter seasons. The remaining cluster represents typical nival regimes where flood events are strongly dominated by the annual snowmelt events.

The same four estimators investigated in the simulation study are applied on this case study with the principal objective of comparing model uncertainties. The stepwise procedure for calibrating nonstationary models resulted in the identification of 21 stations with a time-dependent threshold, 19 stations with a time-dependent mean excess and 3 stations with both time-dependent components, based on a 5% significance level. Overall, nonstationary stations represent 10% of all examined stations. Among them, stations with pluvial or mixed regimes are more likely to be nonstationary (23.5%) (see Table 1). Conversely, the proportion of nonstationary stations with nival regime is 4.9%, which implies that the rejection of the hypothesis of stationarity is similar to random. The spatial distribution of the time-dependent components is illustrated in Figure 3. Stations with a pluvial or mixed regime include 76.2% of the stations with a time-dependent threshold. In particular, 10 of the 13 stations with mixed regimes have positive trends and among the 3 negative trends, 2 of them have a near zero slope with more than 60 years of data. Burn et al. (2016) indicated an increase in the prevalence of rainfall-driven flood events that is coherent with the present findings. At the same time, 13 of the 18 stations (68.4%) with a time-dependent mean excess are located in southern Ontario or southern British Columbia. Across Canada, stations with a time-dependent mean excess are generally negative in a proportion of 2.2 to 1.

4.2 Calibration of a single station

To illustrate the calibration of one station, the stepwise procedure is described in more detail for station 02HL003 located on the Black River, Ontario, which has a mixed flood regime. First, the automatic selection procedure is applied to the stationary at-site model. It leads to a threshold having a significant trend in peak occurrences (p-value of 0.03) according to the logistic regression model. The automatic selection procedure is therefore repeated with a time-dependent threshold. The newly selected time-dependent threshold leads to a trend in the magnitude of the exceedances with a p-value of 0.03 for the Mann-Kendall test. A final run of the automatic selection procedure is performed with both time-dependent components. In this case,, both tests reject the hypothesis of trends.

Outputs of the automatic selection procedure is presented in Figure 5. It reports the estimated GPA shape parameter (denoted “Shape”) and the p-value of the Anderson-Darling test for the threshold candidates. Notice that the selected threshold is associated with 2.48 PPY and corresponds to the first candidate below 2.5 PPY that reaches the maximum p-value of 0.5. The GPA shape parameters associated with the candidate thresholds are relatively stable between approximately 1.4 and 2.8 PPY, but there is a clear evolution below 1.5 PPY. A lot of information would be lost if a threshold lower than 1 PPY was chosen and there is still no clear sign of stability after this point. On the other hand, a p-value of 0.5 indicates strong evidence that the GPA is an appropriate model for the selected threshold, which suggests that in these circumstances the selected threshold is appropriate. Furthermore, Figure 6 assesses the fitting of the mean excess function using the deviance residuals. The top-left panel shows that the average residuals do not diverge substantially from zero. This indicates that the linear trend provides a reasonable description of the persistence in the mean excess. Similarly, the bottom-left panel suggests that the variance function was correctly chosen as it does not diverge substantially from 1. The top-right panel shows the histogram of the standardized exceedances and the bottom-right panel shows the QQ-plot that compares the sample quantiles with the theoretical quantiles of the standardized exceedances. It shows a good agreement between quantiles in the tails of the distribution.

An overall visualization of the model is presented in Figure 7, which includes the estimated time-dependent threshold and mean excess along with the daily streamflow data. A slightly positive slope is reported for the threshold, while the mean excess has a slightly negative slope. Jointly, the flood quantiles of probabilities 0.9 and 0.99, respectively R10 and R100 summarize flood risk for each year. The observed negative slope for R100 shows the relative importance of the mean excess in the evaluation of flood risk. Figure 7 also presents the design levels Q10 and Q100. As expected, the comparison between R10 (R100) and Q10 (Q100) indicates that the design levels behave similarly to an average flood quantile.

4.3 Regional frequency analysis

For each station, a nonstationary index-flood model is set-up following the stepwise procedure. For forming the pooling groups, the calibration of the hierarchical scheme presented in section 2.4 is performed using the transformed mean annual precipitation (MAP) and the drainage area (AREA). Figure 8 reports the results of the leave-one-out cross-validation using a traditional index-flood model (constant growth curve) and the linear predictor of Equation (3) to characterize the GPA shape parameter. The left panel presents for each value of m_0 the minimal cross-validation score. When considering the linear predictor, the results suggest that it is preferable to not impose too severe a restriction on the geographical extent because the selected value is $m_0=350$ and higher m_0 leads to similar scores. It is seen that restricting the geographical distance improves the cross-validation of pooling groups with constant growth curve. In this case $m_0 = 125$ is selected. Overall, Figure 8 shows that the inclusion of the linear predictor improves the modeling of the GPA shape parameter by the members of the pooling groups by about 5%. The right panel of Figure 8 presents the cross-validation score with respect to the final pooling group size (m) for the best m_0. One finds that the best pooling group sizes are respectively 35 and 25.

Once the pooling groups are formed, the four estimators: LMM, MLE, RLM and IND can be evaluated on each pooling group. Bootstrap samples of size 1000 are drawn to obtain an approximate distribution of every model parameter and design level. The relative difference between two estimators in terms of variability is measured by the ratio of their variance. In Figure 9, the variance ratios of each estimation method are compared to the IND method, which corresponds to the denominator and the x-axis represents the GPA shape parameter of the growth curve estimated by the IND method. On the logarithmic scale (base 2), variance ratios below zero indicate that the design levels are estimated with less uncertainty than IND. In particular, values of -1 and 1 indicate that the estimator has half or double the variance of the IND estimates. The first two rows of Figure 9 summarize the comparison between at-site and regional models. This shows that for almost all stations the design levels are estimated more accurately by the regional models. The evaluation of Q100 corresponds to the extrapolation to higher risk than Q10. It is then reasonable to see that the variance ratios associated with Q10 exhibit less spread than Q100. The comparison between the RLM and IND methods shows similar results to the simulation study. Indeed, the IND estimator is found to be in general more accurate than RLM when the GPA shape parameter is outside the interval [-0.1,0.1], while the opposite seems to be true in the present case study. However, note that for both design levels the difference between the regional methods is relatively small in comparison with the difference between the at-site methods. To better understand these scales, notice that a logarithm value of 0.25 corresponds to a standard deviation 9% higher, while a value of 2.5 corresponds to a standard deviation 238% higher.

To understand the impact of selecting a nonstationary index-flood model versus a stationary index flood model, Figure 10 reports the relative difference between the design level estimated by the independent likelihood for both approaches. Note that the GPA shape parameter is a regional estimate and that most stations are stationary, consequently the GPA shape parameter does not differ substantially in both approaches. Figure 10 shows that the nonstationary stations with more than 60 years of data have equal or lower design level in comparison with stationary models with an average of 5%. For the stations with fewer than 60 years of data, the average relative difference is not significantly different from zero according to a Wilcoxon rank-sum test. Several reasons may explain this outcome. As mentioned, for stations with shorter time series, the relative difference between stationary and nonstationary models may not represent a persistent change and may be a consequence of shorter oscillation patterns. Additionally, in this situation the reference period represents a large proportion of the observed years and the design levels of the two approaches may be similar, even if an important trend is observed. Overall, Figure 10 suggests that for sufficiently long time series the replacement of the stationary models by nonstationary models entails smaller flood risk. These results are in agreement with research that shows that due to global warming, the important spring snowmelt events that characterize major floods in a majority of rivers in Canada are expected to occur earlier during the year and drain water from smaller snowpacks (Burn et al., 2016; Cunderlik and Ouarda, 2009).

5. Discussion and Conclusions

A stepwise procedure was introduced to calibrate a nonstationary model using trend tests, L-moments and regression techniques. For this procedure, a time-dependent GPA distribution was separated into a mean excess and a growth curve. This representation, characteristic of index-flood models, allowed the adaptation of existing automatic procedures for selecting threshold exceedances by ensuring the stability of the growth curve. A second benefit of this representation is that mixed pooling groups containing nonstationary and stationary stations were created to resolve the issue of finding stations with similar hydrological properties. Indeed, among 425 stations in Canada, the stepwise procedure led to the consideration of time-dependent components in 10% of the studied stations, although higher concentrations of nonstationary models were found in regions characterized by pluvial and mixed regimes.

A comparison of four estimation methods was carried out in a simulation study. For a single station, the comparison between the regression approach and the maximum likelihood method has shown that design levels derived from the regression approach were generally less biased and more accurate for shorter time series having negative GPA shape parameters (thick-tailed distributions). This suggested that the regression approach could be recommended as a robust strategy to perform at-site frequency analysis. The GPA distribution has a clear variance function that makes the use of quasi-likelihood straightforward in the stepwise procedure. McCullagh and Nelder (1989) mentioned that quasi-likelihood tends to behave similarly to the log-likelihood function. Therefore, it can be argued that the main difference between the regression approach and the maximum likelihood method is the estimation of the GPA shape parameter by the L-moments. Indeed, similar qualities attributed to the regression approach in this study are shared by L-moment estimators in a stationary context (Hosking, 1990).

For the regional model, it was also demonstrated in the simulation study that using the independent likelihood method led to the most accurate estimates of the design levels Q10 and Q100. For the Canadian case study, 43 stations were found to require a time-dependent threshold or mean excess. Using the variance ratios between the four estimation methods it was shown that the estimates provided by the regression approach have a comparable variability level to those of the independent likelihood when the GPA shape parameter is in the interval [-0.1, 0.1]. Although the majority of the stations have a GPA shape parameter in this interval, when the GPA shape parameter is outside this interval, the independent likelihood method was found to reduce model uncertainty. For stations with more than 60 years of data, the comparison of the design levels based on a 30-year period indicated that the utilization of nonstationary models should result in a lower evaluation of the flood risk than stationary models. Luke et al. (2017) put forward the idea of update stationarity, which recommends that flood risk associated with recent years of data be used as a way to predict future flood risks. Further research is necessary to assess if the design levels as defined in this study represent a reliable indicator for that purpose. However, in the meantime, this study shows that a nonstationary index-flood model using pooling groups that mix stationary and nonstationary stations can be recommended to reduce the variability of design levels.

Acknowledgement

This work was supported by the Natural Sciences and Engineering Research Council (NSERC) Canadian FloodNet (# NETGP 451456 – 13). Drainage area and streamflow data are available on the website of the water survey of Canada (https://wateroffice.ec.gc.ca/search/historical_e.html). Mean annual precipitation was provided by Environment and Climate Change Canada (ECCC). A special thanks to Dr. Shabnam Motofi Zadeh for its help with collecting the data.

References

Bezak, N., Brilly, M., Šraj, M., 2014. Comparison between the peaks-over-threshold method and the annual maximum method for flood frequency analysis. Hydrological Sciences Journal 59, 959–977. https://doi.org/10.1080/02626667.2013.831174

Blöschl, G., Ardoin-Bardin, S., Bonell, M., Dorninger, M., Goodrich, D., Gutknecht, D., Matamoros, D., Merz, B., Shand, P., Szolgay, J., 2007. At what scales do climate variability and land cover change impact on flooding and low flows? Hydrological Processes 21, 1241–1247. https://doi.org/10.1002/hyp.6669

Burn, D.H., 1990. An appraisal of the "region of influence" approach to flood frequency analysis. Hydrological Sciences Journal 35, 149–165. https://doi.org/10.1080/02626669009492415

Burn, D.H., Whitfield, P.H., Sharif, M., 2016. Identification of changes in floods and flood regimes in Canada using a peaks over threshold approach. Hydrol. Process. 30, 3303–3314. https://doi.org/10.1002/hyp.10861

Chebana, F., Ouarda, T.B.M.J., 2009. Index flood–based multivariate regional frequency analysis. Water Resources Research 45. https://doi.org/10.1029/2008WR007490

Choulakian, V., Stephens, M.A., 2001. Goodness-of-Fit Tests for the Generalized Pareto Distribution. Technometrics 43, 478–484. https://doi.org/10.2307/1270819

Coles, S., 2001. An introduction to statistical modeling of extreme values. Springer Verlag.

Cooley, D., 2013. Return Periods and Return Levels Under Climate Change, in: Extremes in a Changing Climate, Water Science and Technology Library. Springer, Dordrecht, pp. 97–114. https://doi.org/10.1007/978-94-007-4479-0_4

Cunderlik, J.M., Ouarda, T.B.M.J., 2009. Trends in the timing and magnitude of floods in Canada. Journal of Hydrology 375, 471–480. https://doi.org/10.1016/j.jhydrol.2009.06.050

Cunnane, C., 1973. A particular comparison of annual maxima and partial duration series methods of flood frequency prediction. Journal of Hydrology 18, 257–271. https://doi.org/10.1016/0022-1694(73)90051-6

Davison, A.C., Padoan, S.A., Ribatet, M., 2012. Statistical Modeling of Spatial Extremes. Statist. Sci. 27, 161–186. https://doi.org/10.1214/11-STS376

Davison, A.C., Smith, R.L., 1990. Models for Exceedances over High Thresholds. Journal of the Royal Statistical Society. Series B (Methodological) 52, 393–442.

Durocher, M., Burn, D.H., Mostofi Zadeh, S., 2018a. A nationwide regional flood frequency analysis at ungauged sites using ROI/GLS with copulas and super regions. Journal of Hydrology 567, 191–202. https://doi.org/10.1016/j.jhydrol.2018.10.011

Durocher, M., Zadeh, S.M., Burn, D.H., Ashkar, F., 2018b. Comparison of automatic procedures for selecting flood peaks over threshold based on goodness-of-fit tests. Hydrological Processes 0. https://doi.org/10.1002/hyp.13223

El Adlouni, S., Ouarda, T.B.M.J., Zhang, X., Roy, R., Bobée, B., 2007. Generalized maximum likelihood estimators for the nonstationary generalized extreme value model. Water Resources Research 43. https://doi.org/10.1029/2005WR004545

Eng, P. C. Milly, Gary D. Tasker, 2007. Flood Regionalization: A Hybrid Geographic and Predictor-Variable Region-of-Influence Regression Method. Journal of Hydrologic Engineering 12, 585–591. https://doi.org/10.1061/(ASCE)1084-0699(2007)12:6(585)

Frei, C., Schär, C., 2001. Detection Probability of Trends in Rare Events: Theory and Application to Heavy Precipitation in the Alpine Region. J. Climate 14, 1568–1584. https://doi.org/10.1175/1520-0442(2001)014<1568:DPOTIR>2.0.CO;2

GREHYS, 1996. Presentation and review of some methods for regional flood frequency analysis. Journal of Hydrology 186, 63–84. https://doi.org/10.1016/S0022-1694(96)03042-9

Hall, J., Arheimer, B., Borga, M., Brázdil, R., Claps, P., Kiss, A., Kjeldsen, T.R., Kriaučiūnienė, J., Kundzewicz, Z.W., Lang, M., Llasat, M.C., Macdonald, N., McIntyre, N., Mediero, L., Merz, B., Merz, R., Molnar, P., Montanari, A., Neuhold, C., Parajka, J., Perdigão, R. a. P., Plavcová, L., Rogger, M., Salinas, J.L., Sauquet, E., Schär, C., Szolgay, J., Viglione, A., Blöschl, G., 2014. Understanding flood regime changes in Europe: a state-of-the-art assessment. Hydrology and Earth System Sciences 18, 2735–2772. https://doi.org/10.5194/hess-18-2735-2014

Hanel, M., Buishand, T.A., Ferro, C.A.T., 2009. A nonstationary index flood model for precipitation extremes in transient regional climate model simulations. Journal of Geophysical Research: Atmospheres 114. https://doi.org/10.1029/2009JD011712

Helsel, D.R., Hirsch, R.M., 2002. Statistical Methods in Water Resources, in: Techniques of Water-Resources Investigations of the United States Geological Survey.

Hosking, J.R.M., 1990. L-Moments: Analysis and Estimation of Distributions Using Linear Combinations of Order Statistics. Journal of the Royal Statistical Society. Series B (Methodological) 52, 105–124.

Hosking, J.R.M., Wallis, J.R., 1997. Regional frequency analysis: an approach based on L-moments. Cambridge Univ Pr.

Katz, R.W., 2013. Statistical Methods for Nonstationary Extremes, in: Extremes in a Changing Climate, Water Science and Technology Library. Springer, Dordrecht, pp. 15–37. https://doi.org/10.1007/978-94-007-4479-0_2

Kiem, A.S., Franks, S.W., Kuczera, G., 2003. Multi-decadal variability of flood risk. Geophysical Research Letters 30. https://doi.org/10.1029/2002GL015992

Koenker, R., Bassett, G., 1978. Regression Quantiles. Econometrica 46, 33–50. https://doi.org/10.2307/1913643

Koutsoyiannis, D., 2005. Hydrologic Persistence and The Hurst Phenomenon, in: Water Encyclopedia. John Wiley & Sons, Inc. https://doi.org/10.1002/047147844X.sw434

Kundzewicz, Z.W., 2012. Changes in Flood Risk in Europe, CRC Press. ed.

Kyselý, J., Picek, J., Beranová, R., 2010. Estimating extremes in climate change simulations using the peaks-over-threshold method with a non-stationary threshold. Global and Planetary Change 72, 55–68. https://doi.org/10.1016/j.gloplacha.2010.03.006

Lang, M., Ouarda, T.B.M.J., Bobée, B., 1999. Towards operational guidelines for over-threshold modeling. Journal of Hydrology 225, 103–117. https://doi.org/10.1016/S0022-1694(99)00167-5

Luke, A., Vrugt, J.A., AghaKouchak, A., Matthew, R., Sanders, B.F., 2017. Predicting nonstationary flood frequencies: Evidence supports an updated stationarity thesis in the

United States. Water Resources Research 53, 5469–5494. https://doi.org/10.1002/2016WR019676

Madsen, H., Rasmussen, P.F., Rosbjerg, D., 1997. Comparison of annual maximum series and partial duration series methods for modeling extreme hydrologic events: 1. At-site modeling. Water Resour. Res. 33, 747–757. https://doi.org/10.1029/96WR03848

Madsen, H., Rosbjerg, D., 1997. The partial duration series method in regional index-flood modeling. Water Resources Research 33, 737–746. https://doi.org/10.1029/96WR03847

McCullagh, P., Nelder, J.A., 1989. Generalized linear models. Monographs on Statistics and Applied Probability 37. Chapman Hall, London.

Mediero, L., Kjeldsen, T.R., Macdonald, N., Kohnova, S., Merz, B., Vorogushyn, S., Wilson, D., Alburquerque, T., Blöschl, G., Bogdanowicz, E., Castellarin, A., Hall, J., Kobold, M., Kriauciuniene, J., Lang, M., Madsen, H., Onuşluel Gül, G., Perdigão, R.A.P., Roald, L.A., Salinas, J.L., Toumazis, A.D., Veijalainen, N., Þórarinsson, Ó., 2015. Identification of coherent flood regions across Europe by using the longest streamflow records. Journal of Hydrology 528, 341–360. https://doi.org/10.1016/j.jhydrol.2015.06.016

Montanari, A., Koutsoyiannis, D., 2014. Modeling and mitigating natural hazards: Stationarity is immortal! Water Resources Research 50, 9748–9756. https://doi.org/10.1002/2014WR016092

Mostofi Zadeh, S., Durocher, M., Burn, D.H., Ashkar, F., 2019. Pooled flood frequency analysis: a comparison based on peaks-over-threshold and annual maximum series. Hydrological Sciences Journal 0, null. https://doi.org/10.1080/02626667.2019.1577556

Northrop, P.J., Jonathan, P., 2011. Threshold modelling of spatially dependent non-stationary extremes with application to hurricane-induced wave heights. Environmetrics 22, 799–809. https://doi.org/10.1002/env.1106

O'Brien, N.L., Burn, D.H., 2014. A nonstationary index-flood technique for estimating extreme quantiles for annual maximum streamflow. Journal of Hydrology 519, 2040–2048. https://doi.org/10.1016/j.jhydrol.2014.09.041

Önöz, B., Bayazit, M., 2012. Block bootstrap for Mann–Kendall trend test of serially dependent data. Hydrol. Process. 26, 3552–3560. https://doi.org/10.1002/hyp.8438

Padoan, S.A., Ribatet, M., Sisson, S.A., 2010. Likelihood-Based Inference for Max-Stable Processes. Journal of the American Statistical Association 105, 263–277. https://doi.org/10.1198/jasa.2009.tm08577

Prosdocimi I., Kjeldsen T. R., Miller J. D., 2015. Detection and attribution of urbanization effect on flood extremes using nonstationary flood-frequency models. Water Resources Research 51, 4244–4262. https://doi.org/10.1002/2015WR017065

Renard, B., Lall, U., 2014. Regional frequency analysis conditioned on large-scale atmospheric or oceanic fields. Water Resour. Res. 50, 9536–9554. https://doi.org/10.1002/2014WR016277

Renard, B., Sun, X., Lang, M., 2013. Bayesian Methods for Non-stationary Extreme Value Analysis, in: AghaKouchak, A., Easterling, D., Hsu, K., Schubert, S., Sorooshian, S.

(Eds.), Extremes in a Changing Climate: Detection, Analysis and Uncertainty, Water Science and Technology Library. Springer Netherlands, Dordrecht, pp. 39–95. https://doi.org/10.1007/978-94-007-4479-0_3

Requena, A.I., Chebana, F., Mediero, L., 2016. A complete procedure for multivariate index-flood model application. Journal of Hydrology 535, 559–580. https://doi.org/10.1016/j.jhydrol.2016.02.004

Robson, A., Reed, D., 1999. Flood estimation handbook. Institute of Hydrology, Wallingford.

Roth, M., Buishand, T.A., Jongbloed, G., Tank, A.M.G.K., Zanten, J.H. van, 2012. A regional peaks-over-threshold model in a nonstationary climate. Water Resources Research 48. https://doi.org/10.1029/2012WR012214

Salas, J.D., Obeysekera, J., Vogel, R.M., 2018. Techniques for assessing water infrastructure for nonstationary extreme events: a review. Hydrological Sciences Journal 63, 325–352. https://doi.org/10.1080/02626667.2018.1426858

Serago, J.M., Vogel, R.M., 2018. Parsimonious nonstationary flood frequency analysis. Advances in Water Resources 112, 1–16. https://doi.org/10.1016/j.advwatres.2017.11.026

Serinaldi, F., Kilsby, C.G., 2015. Stationarity is undead: Uncertainty dominates the distribution of extremes. Advances in Water Resources 77, 17–36. https://doi.org/10.1016/j.advwatres.2014.12.013

Solari, S., Egüen, M., Polo, M.J., Losada, M.A., 2017. Peaks Over Threshold (POT): A methodology for automatic threshold estimation using goodness of fit p-value. Water Resour. Res. 53, 2833–2849. https://doi.org/10.1002/2016WR019426

Sun, X., Thyer, M., Renard, B., Lang, M., 2014. A general regional frequency analysis framework for quantifying local-scale climate effects: A case study of {ENSO} effects on Southeast Queensland rainfall. Journal of Hydrology 512, 53–68. http://dx.doi.org/10.1016/j.jhydrol.2014.02.025

Tasker, G.D., Hodge, S.A., Barks, C.S., 1996. Region of Influence Regression for Estimating the 50-Year Flood at Ungaged Sites1. JAWRA Journal of the American Water Resources Association 32, 163–170. https://doi.org/10.1111/j.1752-1688.1996.tb03444.x

Thibaud, E., Mutzner, R., Davison, A.C., 2013. Threshold modeling of extreme spatial rainfall. Water Resources Research 49, 4633–4644. https://doi.org/10.1002/wrcr.20329

USGS, 2018. Guidelines for determining flood flow frequency—Bulletin 17C.

Varin, C., Reid, N., Firth, D., 2011. An overview of composite likelihood methods. Statistica Sinica 21, 5–42.

Viglione, A., Merz, B., Dung, N.V., Parajka, J., Nester, T., Blöschl, G., 2016. Attribution of regional flood changes based on scaling fingerprints. Water Resources Research 52, 5322–5340. https://doi.org/10.1002/2016WR019036

Villarini, G., Smith, J.A., Napolitano, F., 2010. Nonstationary modeling of a long record of rainfall and temperature over Rome. Advances in Water Resources, Special Issue on

Novel Insights in Hydrological Modelling 33, 1256–1267. https://doi.org/10.1016/j.advwatres.2010.03.013

Villarini, G., Smith, J.A., Serinaldi, F., Bales, J., Bates, P.D., Krajewski, W.F., 2009. Flood frequency analysis for nonstationary annual peak records in an urban drainage basin. Advances in Water Resources 32, 1255–1266. https://doi.org/10.1016/j.advwatres.2009.05.003

Vogel, R.M., Yaindl, C., Walter, M., 2011. Nonstationarity: Flood Magnification and Recurrence Reduction Factors in the United States1. JAWRA Journal of the American Water Resources Association 47, 464–474. https://doi.org/10.1111/j.1752-1688.2011.00541.x

Wang, Z., Yan, J., Zhang, X., 2014. Incorporating spatial dependence in regional frequency analysis. Water Resour. Res. 50, 9570–9585. https://doi.org/10.1002/2013WR014849

Ward, J.H., 1963. Hierarchical Grouping to Optimize an Objective Function. Journal of the American Statistical Association 58, 236–244. https://doi.org/10.1080/01621459.1963.10500845

WSC, 2018. Water Survey of Canada [WWW Document]. URL http://www.wsc.ec.gc.ca/applications/H2O/index-eng.cfm

Tables

Table 1: Contingency table of the selected stations by type of time-dependent components (trend) used.

	Record length			Regime			Slope		
Trend	**40-**	**40-60**	**60+**	**Pluvial**	**Mixed**	**Nival**	**Negative**	**Positive**	**Total**
Threshold	4	12	5	3	13	5	8	13	21
Mean excess	4	10	5	5	8	6	13	6	19
Both	1	1	1	0	2	1	2	1	3
Stationary	125	192	65	25	107	247	-	-	382
Total	134	215	76	32	130	259	-	-	425

Note: Sign of the slope for "Both" is based on the slope of the mean excess.

Figures

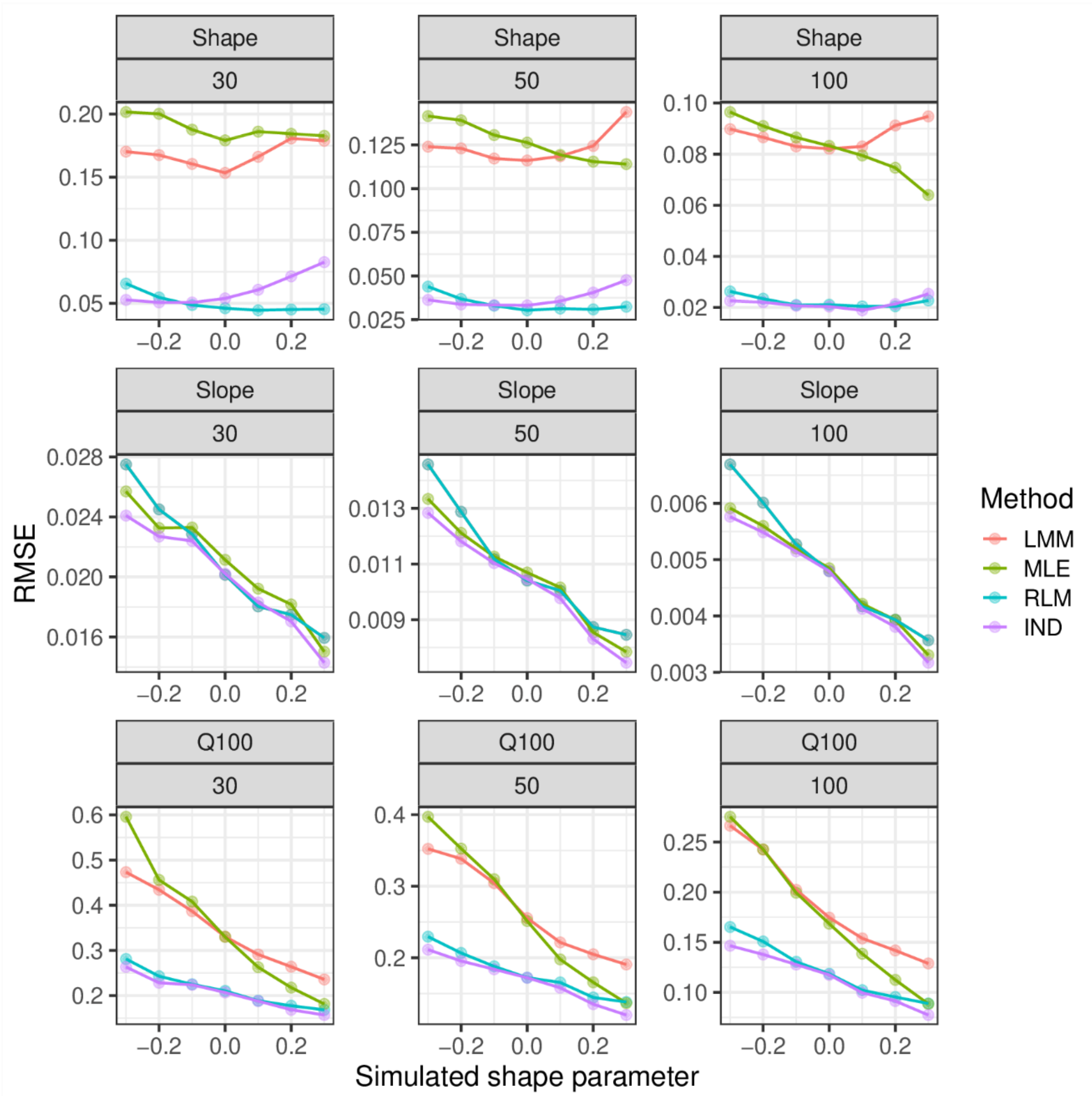

Figure 1: Root mean square errors of the four estimators considered in the simulation study. Each panel is associated with a parameter or design level derived from the nonstationary index-flood model. Record lengths of 30, 50 and 100 years are reported.

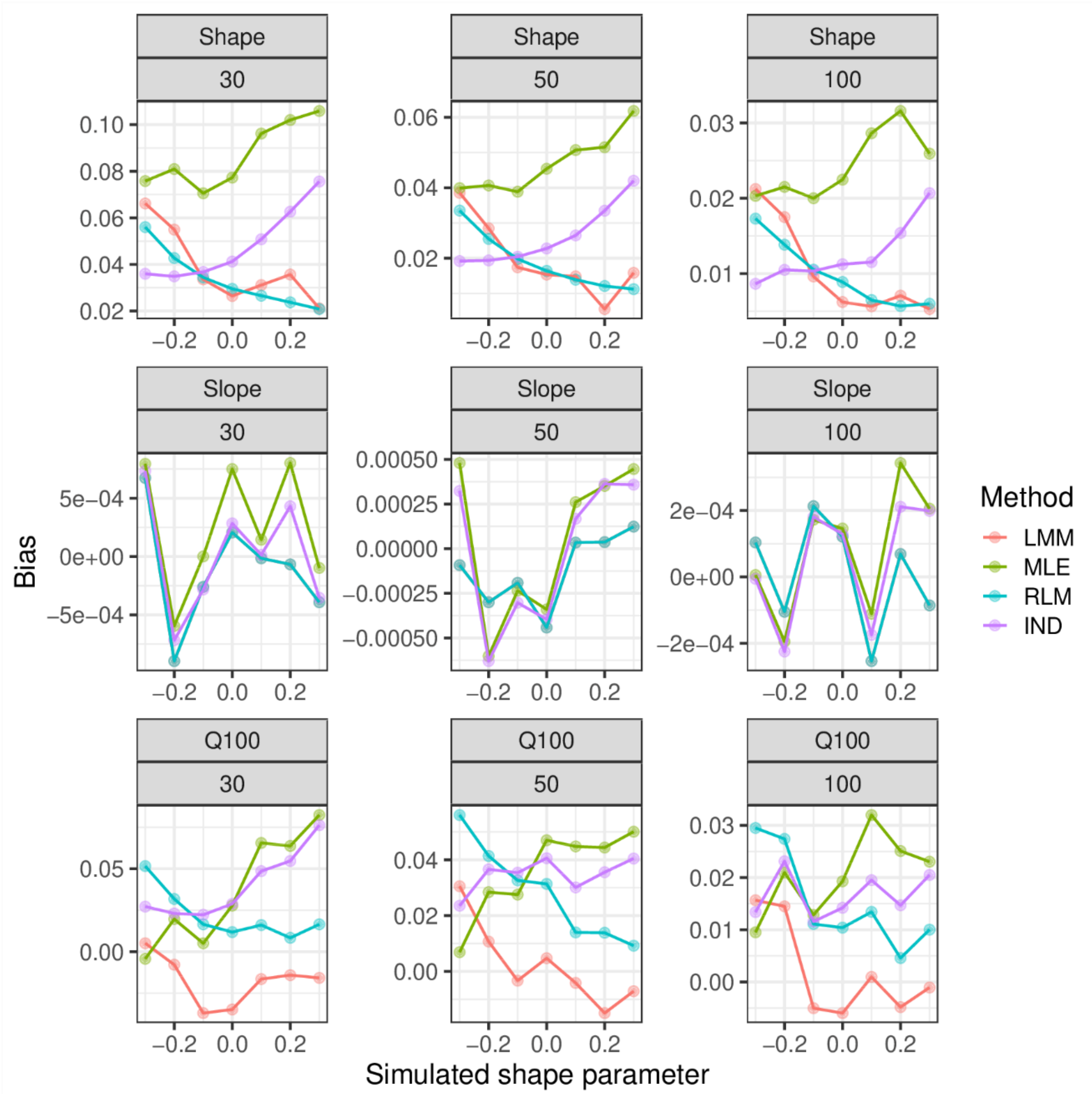

Figure 2: Bias of the four estimators considered in the simulation study. See Figure 1 for details.

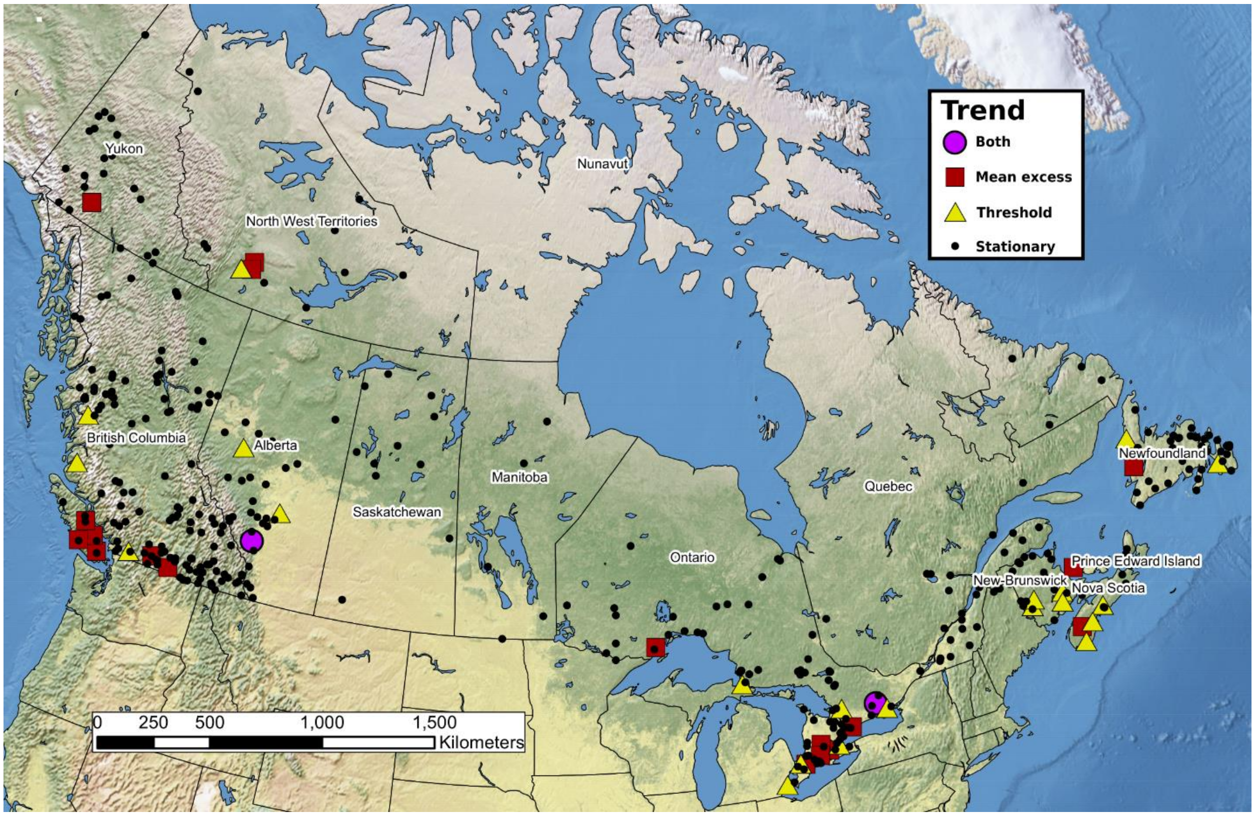

Figure 3: Locations of the 425 stations by the type of time-dependent component (trend).

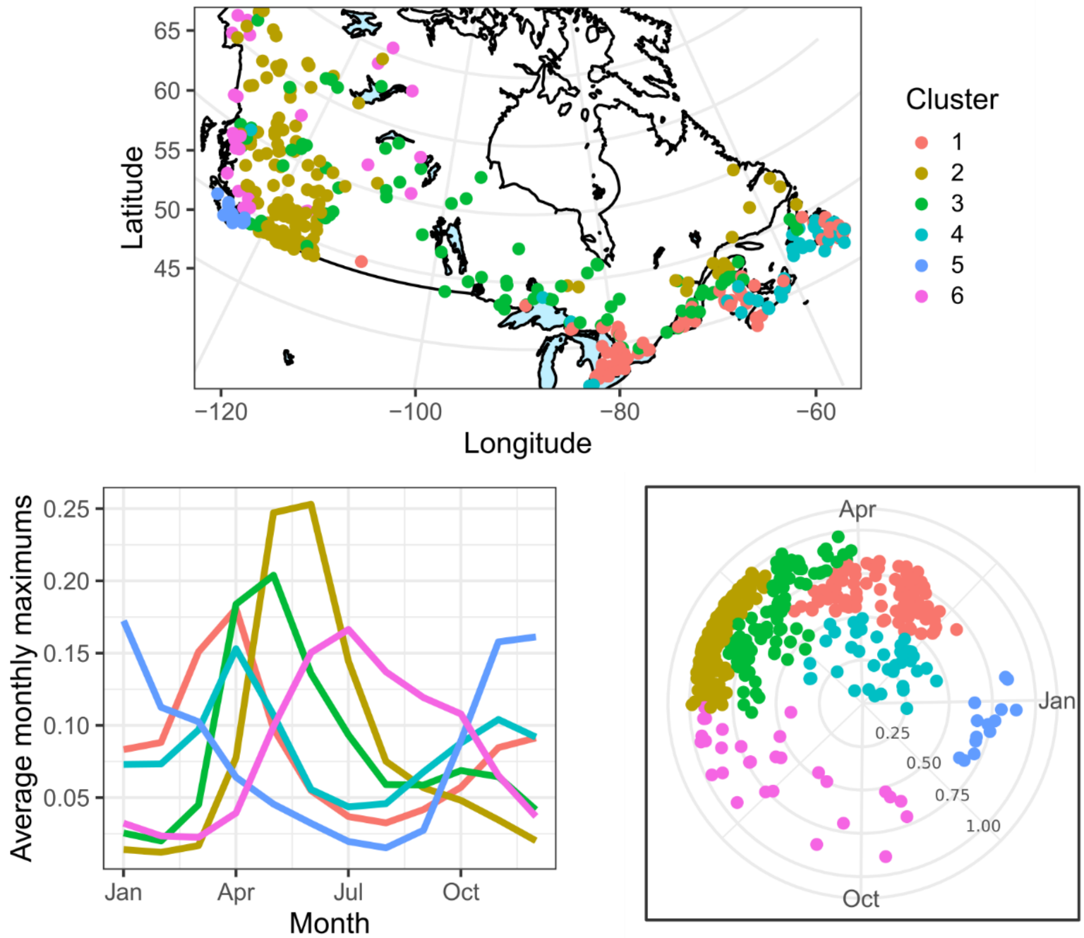

Figure 4: Classification of the stations in the seasonal space. The panels show respectively the location, average monthly maximum flow and position in the seasonal space of the stations.

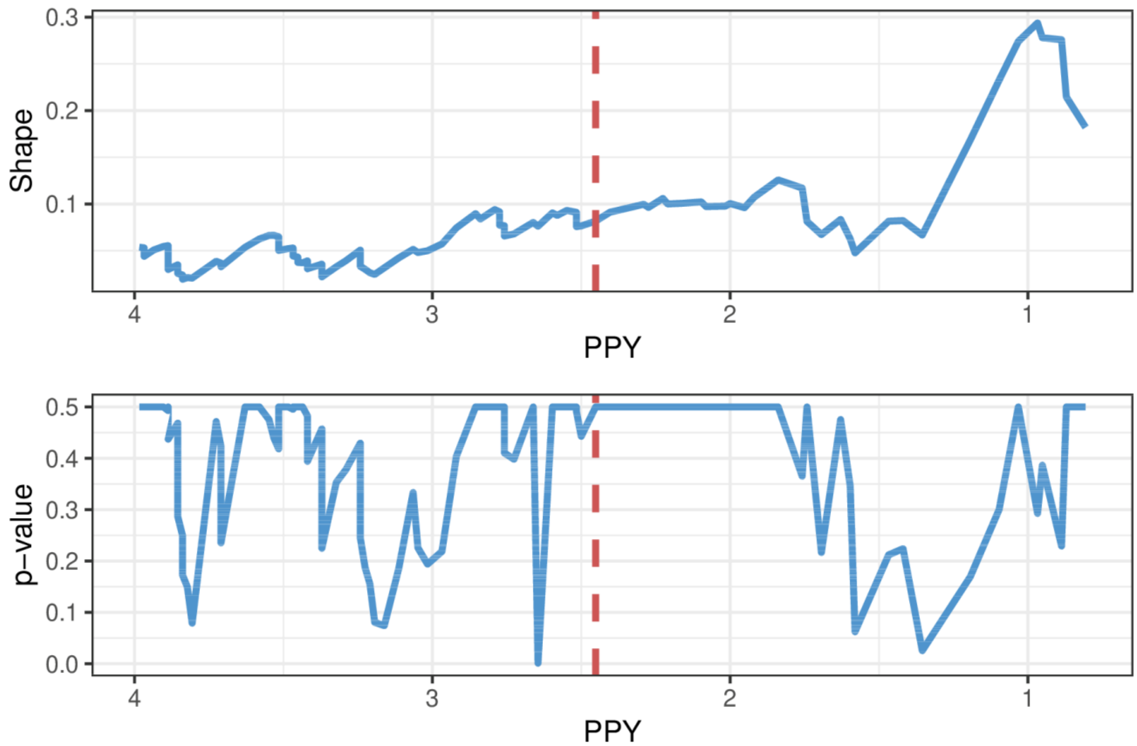

Figure 5: Visual diagnostics for selecting the threshold of station 02HL003. The automatically selected threshold is indicated by the dashed line.

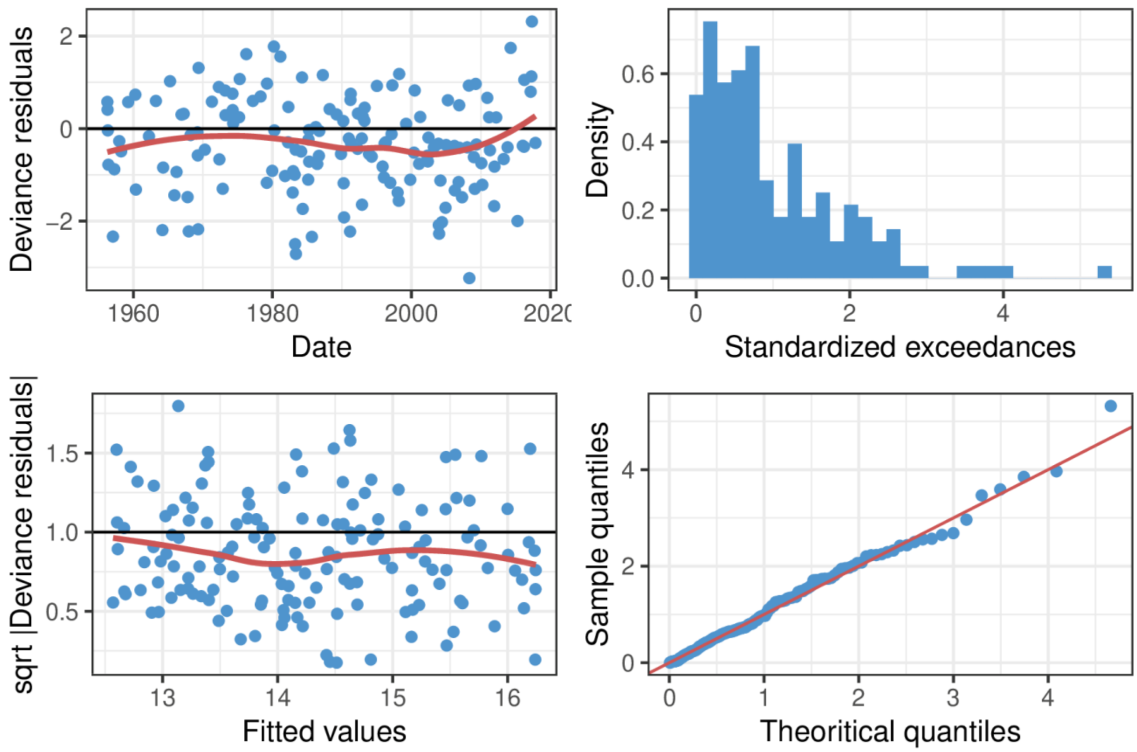

Figure 6: Regression diagnostics for the mean excess of station 02HL003.

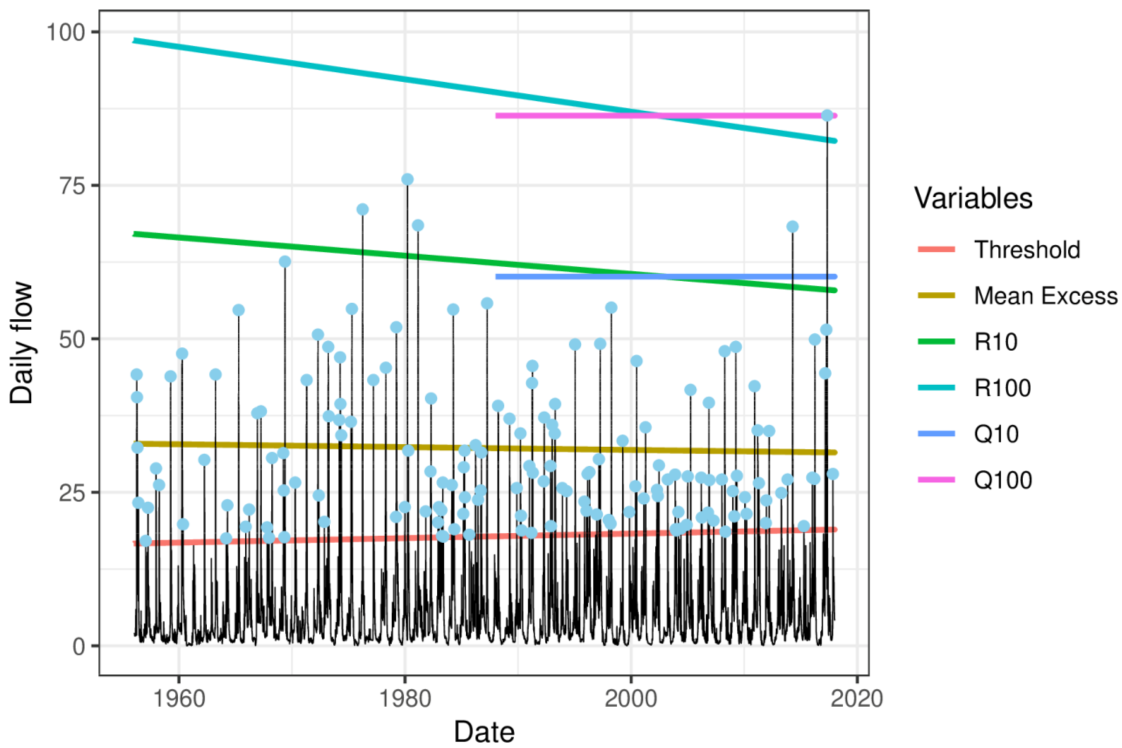

Figure 7: Daily flow series of station 02HL003 with time-dependent components of the nonstationary index-flood model.

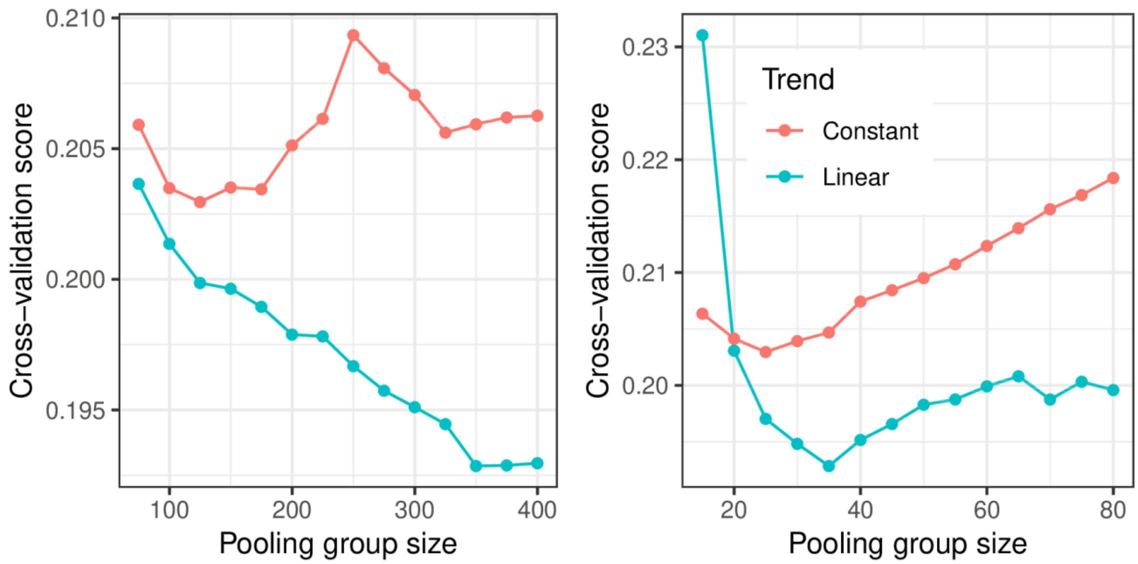

Figure 8 : Cross-validation scores for the formation of the pooling group using hierarchical distances. At left, the minimal cross-validation scores in respect of geographical distance (m_0). At right, pooling group sizes (m) for best scores in left panel. For the red line, the pooling groups are using a constant GPA shape parameter and for the blue line, the pooling groups are using a linear predictor to characterize the GPA shape parameter.

847

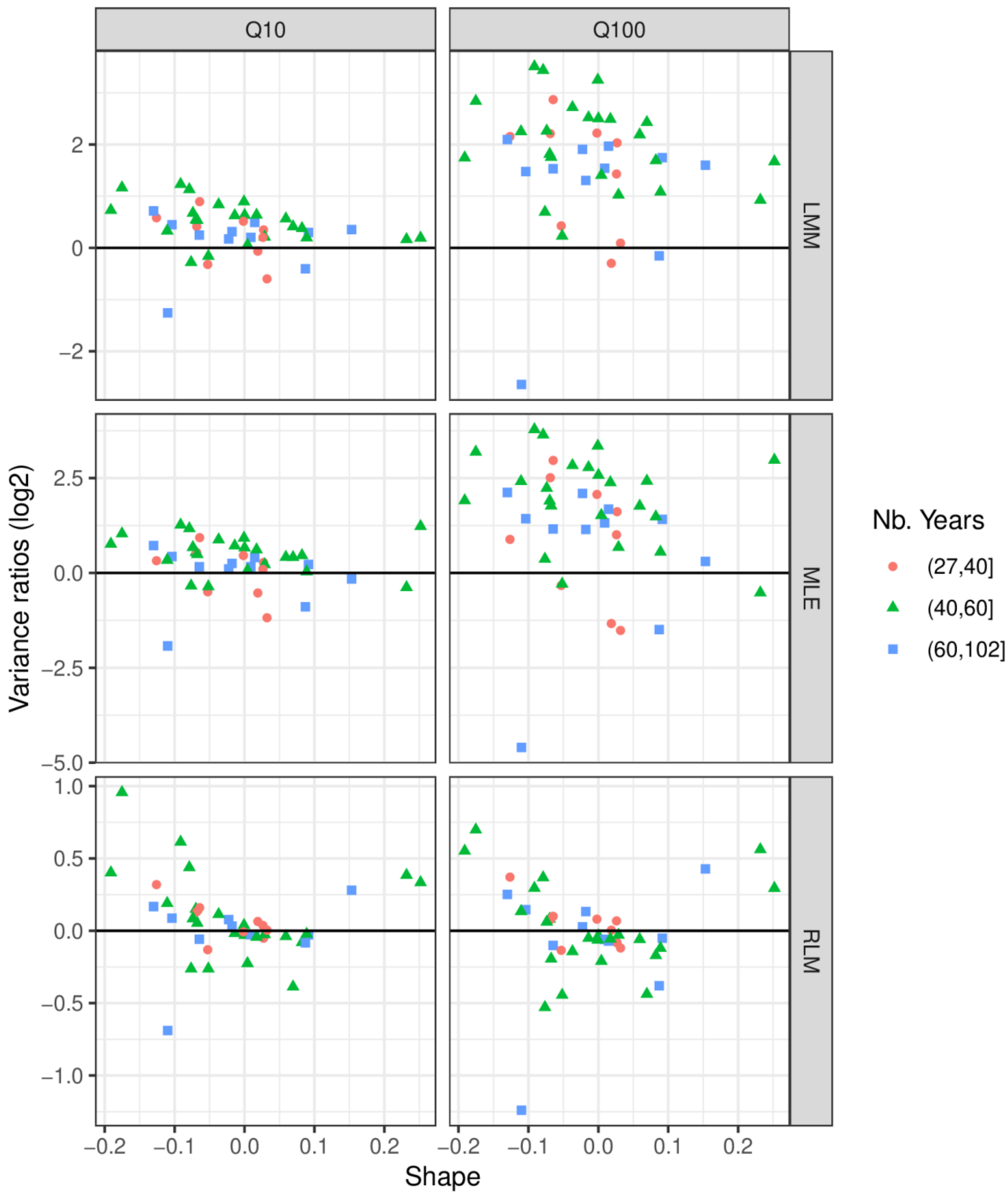

848

849 **Figure 9: Variance ratios of the four estimation methods applied on 43 nonstationary**
850 **stations in Canada. The independence likelihood estimator (IND) is used as a benchmark**
851 **(denominator).**

852

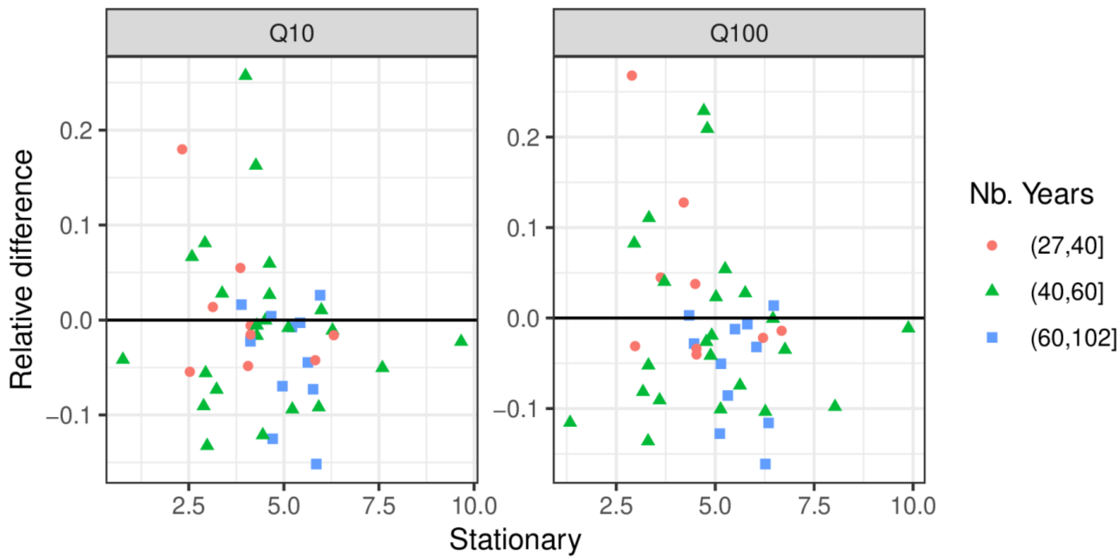

Figure 10: Relative difference between design levels from stationary and nonstationary models with respect to stationary design levels for 43 nonstationary stations in Canada. The design levels are transformed to the logarithm scale and the differences are standardized by the stationary design levels. The estimates are obtained by the independent likelihood method.